UDC 621.396.96:629.12
DOI: 10.20535/SRIT.2308-8893.2024.2.03

POLARIZATION-BASED TARGET DETECTION APPROACH TO ENHANCE SMALL SURFACE OBJECT IDENTIFICATION ENSURING NAVIGATION SAFETY

M. STETSENKO, O. MELNYK, I. VOROKHOBIN, D. KORBAN, O. ONISHCHENKO, V. TERNOVSKY, I. IVANOVA

Abstract. This research introduces a groundbreaking approach to significantly enhance the performance of navigation radars under adverse weather conditions. Traditional ship radars, relying on horizontal polarization, encounter difficulties in effectively suppressing rain interference. In response, this study proposed an innovative method employing circular polarization for detecting navigation targets. This technique capitalizes on the distinct polarization properties exhibited by stable navigation targets and fluctuating interfering objects. Theoretical analysis and model experiments substantiate consistent ellipticity parameter values of scattered waves, independent of rain intensity, for both rain interferers and surface metallic objects. The practical implications of our research are highly promising. They enable detection irrespective of the noise-to-signal ratio by integrating an additional channel of circularly polarized waves and applying straightforward mathematical functions. This advancement marks a significant stride towards overcoming the challenges posed by rainy conditions in maritime navigation radar systems.

Keywords: safety of shipping, navigational safety, maritime transportation, radar interference, unfavorable weather conditions, rain and snow interference suppression, navigational targets, automonous surface vehicles, radiolocation principles, ship detection principles framework, radar accuracy.

INTRODUCTION

In today's global transportation landscape, approximately 80% of cargo is transported via oceangoing vessels, constituting a fleet of nearly 100 thousand units. Given this extensive maritime activity, ensuring navigation safety is paramount and involves adherence to specific technical requisites and construction guidelines. Central to these regulations is the inclusion of a navigation radar as standard equipment aboard seagoing vessels, serving as a critical tool for safeguarding navigation. The operator's ability to make precise decisions regarding vessel positioning, collision avoidance, and grounding prevention hinges significantly on the accuracy of radar-derived data.

Regrettably, the quality of data received is not consistently optimal. Operators frequently encounter challenges, particularly in adverse weather conditions such as heavy seas, rain, and snow. These atmospheric conditions introduce interference that affects radar performance. Presently, there exist various methods to mitigate rain and snow interference. The hardware approach employs a gain function, enabling operators to manually adjust signal strength to filter out low-amplitude signals. However, this manual intervention often results in unintended consequences, potentially filtering useful signals from small surface targets like small boats and floating objects.

To address this dilemma, contemporary radars employ algorithms designed to suppress rain and snow interference. Typically, interference from precipitation follows an even distribution pattern. The intensity of interference correlates with the severity of rain or snowfall. This interference can be effectively suppressed using a Constant False Alarm Rate (CFAR) approach. In low-resolution radars, the interference probability density aligns with a Rayleigh distribution. In high-resolution radars, it can be modeled by a Weibull distribution.

The CFAR mechanism enables the adjustment of interference control thresholds, allowing for a specified false alarm rate and enhancing target tracking capabilities. However, in scenarios where substantial noise fluctuations occur, the likelihood of false alarms rises. To sustain a consistent false alarm rate, it becomes imperative to elevate the detection threshold proportionally, subsequently augmenting the input signal-to-noise ratio. This adaptation, while crucial, does introduce a trade-off in the form of a potential loss of the consistent false alarm rate (LCFAR).

The literature review encompasses a diverse array of sources that significantly contribute to the radar technology field. Bohren and Huffman's seminal work, "Absorption and Scattering of Light by Small Particles" (1998), provides fundamental insights into the behavior of light with small particles. Their earlier 1983 paper underscores their enduring impact in the field. Reference [2] introduces a signal processing algorithm specifically tailored for ship navigation radar, with a focus on azimuth distance monitoring. Scientific work [3] delves into polarization invariants within the scattering matrix, emphasizing stability in aperture synthesis. Paper [4] critically distinguishes between forward propagation and backscattering in formulating the proper polarimetric scattering matrix for radar systems. Reference [5] demonstrates the practical application of polarimetric radar technology in target detection through a method based on polarimetric Synthetic Aperture Radar (SAR). Source [6] lays the foundation for understanding radiolocation principles, potentially exploring pivotal concepts and theoretical frameworks. Paper [7] centers on antenna miniaturization for radiolocation, suggesting advancements in antenna technology for enhanced radiolocation applications. Source [8] introduces a novel radiolocation method applicable to depth estimation, with potential applications in groundwater level analysis. Reference [9] discusses beamforming techniques within radio-telescope technology, signifying its relevance in radiolocation applications. Study [10] offers insights into radiolocation experiments within urban environments, potentially addressing challenges specific to this setting. Papers [11; 12] explore the directional radio response of a specific device guided by radiolocation, potentially contributing to advancements in device localization. They also introduce an algorithm for simultaneous radiolocation of multiple sources, indicating advancements in source localization techniques. Works [13; 14] present lightweight radar-based ship detection frameworks, potentially offering innovative methods for ship detection. They propose a unified approach to ship detection, combining optical and radar data, potentially advancing ship detection methods. Source [15] introduces a novel approach for estimating ship speed and heading using radar sequential images, potentially advancing ship tracking technology. Articles [16–18; 43] discuss inshore ship detection methods based on multi-modality saliency, potentially enhancing ship detection accuracy. They present a network designed for small ship detection in synthetic aperture radar imagery, indicating progress in ship detection algorithms. Additionally, they introduce a method for assessing the motion state of

ships and selecting appropriate radar imaging algorithms, potentially improving ship detection accuracy. Source [19] delves into calibration methods involving ground-based, ship-based, and spaceborne radars, potentially enhancing radar accuracy. In [20], the authors focus on estimating ship berthing parameters using a fusion of Multi-LiDAR and MMW radar data, potentially advancing ship docking technology. Articles [21–23] underscore the critical role of situational awareness in ensuring ship safety, addressing the optimization of ship speed for secure heavy cargo transportation under diverse weather conditions, and exploring the concept of autonomous ships and their steering control using mathematical models. Works [24–27] present assessment methodologies based on Markov models for navigational safety, offering a comprehensive approach to evaluating the vulnerability of critical ship equipment and systems. They examine information security risks in shipping to ensure safety in maritime transportation and investigate the environmental impact of ship operation in relation to efficient freight transportation. In [28–30], discussions encompass the use of fuzzy controllers in ship motion control systems for automation, the identification of energy-efficient operation modes for propulsion electrical motors in autonomous swimming apparatus, and the presentation of a straightforward technique for identifying parameters of vessel models.

Papers [31–33] introduce a decision support system concept for designing combined propulsion systems, explore challenges in creating energy-efficient positioning systems for multipurpose sea vessels, and investigate risk management mechanisms in higher education institutions using innovative project information support. Work [34] discusses a method for managing human resources in educational projects of higher education institutions. The article [35] focuses on modeling the creation of organizational energy-entropy. In [36], a model for creating a roadmap for enterprise development is constructed and analyzed. In [37], the dynamics of project portfolio structure in organizational development are examined, considering information entropy resistance. A model depicting the energy entropy dynamics of organizations is constructed and investigated in [38]. Studies on various forms of cooperation among participants in inland waterways cargo delivery in the Dnieper region and the development of a strategy for modernizing passenger ships by optimizing fund distribution are presented in [39; 40].

Recent advancements in system research and information technologies highlight significant developments across various domains where [41] introduced a novel modified kernel fuzzy c-means algorithm to enhance the detection of cotton leaf spots, demonstrating improved accuracy in agricultural diagnostics. The authors in [42] developed a multi-level decision-making framework for predicting and recommending treatments for heart-related diseases, providing a robust tool for healthcare applications. The work [43] proposed an interval type-2 generalizing fuzzy model for monitoring the states of complex systems using expert knowledge and [44; 45] applied optimal set partitioning theory to solve problems in artificial intelligence and pattern recognition, advancing methodologies in AI research.

In light of the aforementioned considerations, the research aims to enhance radar detection of navigation entities amidst atmospheric precipitation, irrespective of its intensity. A novel approach is proposed, focusing on recognizing and categorizing the polarization attributes of partially polarized waves to augment the information capacity of electromagnetic waves. This approach draws from

successful applications of statistical methods in the polarization analysis of rain clouds and precipitation, providing a basis for extending this methodology to the complex task of detecting and tracking intricate objects. By "complex object", we refer to a navigational entity situated against a backdrop of spatially dispersed reflectors that remain consistent throughout radar observations. The primary objective of this study is to establish a statistical correlation between the invariant characteristics of a polarized electromagnetic wave and an object on the sea surface, enveloped by spatially distributed reflectors like rain or other forms of precipitation. Resolving this requires determining the Stokes parameters for the scattered wave upon irradiation of the complex object. This transition from the energy traits to informative parameters such as polarization degree, azimuth, and ellipticity of the polarized wave holds significant promise.

MATERIALS AND METHODS

To describe all possible polarization states of a quasimonochromatic plane wave, four Stokes parameters can be used, which are determined through the components of the transverse electric field.

Let us write the electric vector of a plane monochromatic homogeneous wave in the form

$$\vec{E} = [E_x\ E_y\ ] = 2\left[\left(A_x e^{i(\omega\left(t-\frac{z}{\nu)+\varphi_x}\right)}\right)\left(A_y e^{i\left(\omega(t-\frac{z}{\nu)+\varphi_y}\right)}\right)\right],$$

where A_x, A_y denote amplitudes, and φ_x, φ_y denote phases of the components of plane wave.

Time-averaged values for the amplitude and phase of the parallel and transverse components of the vector $\vec{E}$ determine the known Stokes parameters I, Q, U, V:

$$I = |E_x|^2 + |E_y|^2 = A_x^2(t) + A_y^2(t),$$

$$Q = |E_x|^2 - |E_y|^2 = A_x^2(t) - A_y^2(t),$$

$$U = (E_x E_y^* + E_y E_x^*) = 2\,A_x(t)A_y(t)\text{coscos}[\varphi_x(t) - \varphi_y(t)]\ ,$$

$$V = i(E_x E_y^* - E_y E_x^*) = 2\,A_x(t)A_y(t)\sin[\varphi_x(t) - \varphi_y(t)],$$

where the * sign means the complex conjugate, and the angle brackets mean time averaging: $A_x^2(t) = \frac{1}{T}\int_0^T (t)\,dt\ldots$.

The first component of the Stokes vector I characterizes the intensity of the light flux, the second component Q characterizes the degree of polarization (Fig. 1) [1; 2]. V component defines the direction of rotation of the polarization ellipse: a positive sign means right-handed rotation, and a negative sign means left-handed. The components of the Stokes vector are associated with ellipsometric parameters and have the following properties:

$$I \geq 0,\ I \geq \sqrt{Q^2 + U^2 + V^2}\ ,$$

$$\mathrm{tg}2\gamma = \frac{U}{Q};\quad \mathrm{tg}\,2\eta = \frac{V}{\sqrt{Q^2 + U^2}},$$

where γ is the azimuth; $|tg\eta|$ is the ellipticity of the polarized wave $\left(-\frac{\pi}{4} \leq \eta \leq \frac{\pi}{4}\right)$.

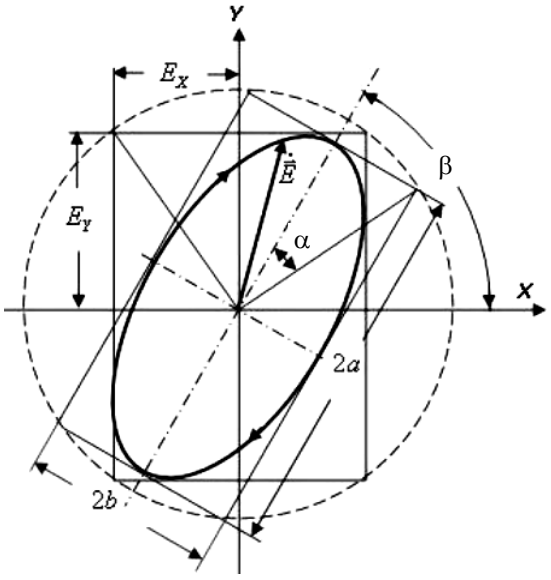

Fig. 1. Polarization ellipse of an electromagnetic wave

It is known that the Stokes parameters of a scattered wave are determined by the Muller scattering matrix. In general terms, the model of scattering of an electromagnetic wave by an arbitrary surface is described by the operator equation:

$$S = M\,S_0,$$

where $S_0 = \{I_0, U_0, V_0, U_0\}^{\mathrm{T}}$ is Stokes vector of incident radiation; $S = \{I, U, V, U\}^{\mathrm{T}}$ is the Stokes vector of scattered radiation; M is the scattering matrix characterizing the reflective properties of the scattering surface and the angle of incidence of the electromagnetic wave [2; 3; 4].

To compose the matrix of the linear scattering operator M, we consider the transformation of the components of the Stokes vector of the incident radiation according to the Fresnel formulas.

The intensities of the incident and scattered radiation are defined as

$$I_0 = \left|E_x^{inc}\right|^2 + \left|E_y^{inc}\right|^2; I = \left|E_x^{refl}\right|^2 + \left|E_y^{refl}\right|^2,$$

where E_x^{inc}, E_y^{inc} are the projections of the vector $\vec{E}^{inc}$ $(\vec{E} = E_x + iE_y)$ on the axis perpendicular to the direction of the incident electromagnetic wave space; alternatively, are the projections of scattered wave.

In turn, the amplitude Fresnel coefficients $\Phi_1 = \frac{E_x^{refl}}{E_x^{inc}}$ and $\Phi_2 = \frac{E_y^{refl}}{E_y^{inc}}$ are equal to the ratio of the amplitudes of the reflected and incident electromagnetic waves parallel and perpendicular to the scattering plane, respectively [4].

For the coefficients Φ_1 and Φ_2 the following expressions are true:

$$\Phi_1 = \frac{m_2 \operatorname{cos}\operatorname{cos}\phi - m_1 \operatorname{cos}\operatorname{cos}\varphi}{m_2 \operatorname{cos}\operatorname{cos}\phi + m_1 \operatorname{cos}\operatorname{cos}\varphi} \frac{m_2 \operatorname{cos}\operatorname{cos}\phi - m_1\sqrt{m_2^2 - (m_1 \operatorname{sin}\operatorname{sin}\phi)^2}}{m_1 \operatorname{cos}\operatorname{cos}\phi + m_1\sqrt{m_2^2 - (m_1 \operatorname{sin}\operatorname{sin}\phi)^2}}, \quad (1)$$

$$\Phi_2 = \frac{m_1 \operatorname{cos}\operatorname{cos}\phi - m_2 \operatorname{cos}\operatorname{cos}\varphi}{m_1 \operatorname{cos}\operatorname{cos}\phi + m_2 \operatorname{cos}\operatorname{cos}\varphi} = \frac{m_1 \operatorname{cos}\operatorname{cos}\phi - m_2\sqrt{m_2^2 - (m_1 \operatorname{sin}\operatorname{sin}\phi)^2}}{m_1 \operatorname{cos}\operatorname{cos}\phi + m_2\sqrt{m_2^2 - (m_1 \operatorname{sin}\operatorname{sin}\phi)^2}}, \quad (2)$$

where m_1 is the complex refractive index of the first medium; m_2 is the complex refractive index of the second medium; ϕ is the angle of incidence of the electromagnetic wave; φ is the angle of refraction of the electromagnetic wave.

Given the law of refraction for the refraction angle φ we write:

$$\operatorname{sin}\operatorname{sin}\varphi = \frac{m_1}{m_2} \operatorname{sin}\operatorname{sin}\phi;$$

$$\operatorname{cos}\operatorname{cos}\varphi = \sqrt{1 - \left(\frac{m_1}{m_2} \operatorname{sin}\operatorname{sin}\phi\right)^2}.$$

Since $E_x^{refl} = \Phi_1 E_x^{inc}$ and $E_y^{refl} = \Phi_2 E_y^{inc}$, it yields

$$I = \left|\Phi_1 E_x^{inc}\right|^2 + \left|\Phi_2 E_y^{inc}\right|^2 = \left|\Phi_1\right|^2 \left|E_x^{inc}\right|^2 + \left|\Phi_2\right|^2 \left|E_y^{inc}\right|^2.$$

Let us express $\left|E_x^{inc}\right|^2$, $\left|E_y^{inc}\right|^2$ through the components I_0, Q_0 of the incident wave Stokes vector. Since $I_0 = \left|E_x\right|^2 + \left|E_y\right|^2$, $Q_0 = \left|E_x\right|^2 - \left|E_y\right|^2$, then

$$\left|E_x^{inc}\right|^2 = \frac{I_0 + Q_0}{2}, \quad \left|E_y^{inc}\right|^2 = \frac{I_0 - Q_0}{2}.$$

Hence,

$$I = \left|\Phi_1\right|^2 \frac{I_0 + Q_0}{2} + \left|\Phi_2\right|^2 \frac{I_0 - Q_0}{2} = \frac{1}{2} I_0 (\left|\Phi_1\right|^2 + \left|\Phi_2\right|^2) + \frac{1}{2} Q_0 (\left|\Phi_1\right|^2 - \left|\Phi_2\right|^2).$$

The second component of the Stokes vector of the scattered radiation is expressed through the components of the Stokes vector of the incident radiation as follows:

$$Q = \left|\Phi_1 E_x^{inc}\right|^2 - \left|\Phi_2 E_y^{inc}\right|^2 = \left|\Phi_1\right|^2 \left|E_x^{inc}\right|^2 - \left|\Phi_2\right|^2 \left|E_y^{inc}\right|^2 =$$

$$= \frac{1}{2} I_0 (\left|\Phi_1\right|^2 - \left|\Phi_2\right|^2) + \frac{1}{2} Q_0 (\left|\Phi_1\right|^2 + \left|\Phi_2\right|^2).$$

We express the third component U of the Stokes vector through the components of the Stokes vector of the incident radiation:

$$U = (\Phi_1\Phi_2^*)U_0 + (\Phi_2\Phi_1^*)V_0 .$$

And finally, for the fourth component of the Stokes vector of reflected radiation, we write

$$V = (\Phi_1\Phi_2^*)U_0 + (\Phi_1\Phi_2^*)V_0 .$$

Thus, for the Stokes vector of scattered radiation, the following expression is obtained:

$$S = \left(\frac{1}{2} I_0 (|\Phi_1|^2 + |\Phi_2|^2) + \frac{1}{2} Q_0 (|\Phi_1|^2 - |\Phi_2|^2) \frac{1}{2} I_0 (|\Phi_1|^2 - |\Phi_2|^2) + \right.$$

$$\left. + \frac{1}{2} Q_0 (|\Phi_1|^2 + |\Phi_2|^2)\ (\Phi_1\Phi_2^*)U_0 + (\Phi_2\Phi_1^*)V_0\ \ (\Phi_1\Phi_2^*)U_0 + (\Phi_1\Phi_2^*)V_0 \right).$$

We compose the Mueller scattering matrix for reflective metal surfaces:

$$M = (M_{11}\, M_{12}\, 0\, 0 M_{21}\, M_{22}\, 0\, 0\, 0\, 0 M_{33}\, M_{34}\, 0\, 0 M_{43}\, M_{44}\ ),$$

where

$$M_{11} = M_{22} = \frac{|\Phi_1|^2 + |\Phi_2|^2}{2}; \quad M_{12} = M_{21} = \frac{|\Phi_1|^2 - |\Phi_2|^2}{2};$$

$$M_{33} = M_{44} = (\Phi_2\Phi_1^*), \ \ M_{34} = -M_{43} = (\Phi_2\Phi_1^*) .$$

Mueller scattering matrix for a raindrop with a spherical shape

It is convenient to decompose the vector of the incident electric field E^{inc} into parallel $E_{|}^{inc}$ and perpendicular $E_{\perp}^{inc}$ components, and present the relationship between the incident and scattered fields in the matrix form:

$$(E_{|}^{refl}\ E_{\perp}^{refl}\ ) = \frac{e^{ik(r-z)}}{-ikr} (S_2\ S_3\ S_4\ S_1\ )(E_{|}^{inc}\ E_{\perp}^{inc}\ ), \tag{3}$$

where k is the wave vector, r is the path travelled by the wave, and S_j $(j = 1, 2, 3, 4)$ are the elements of the amplitude scattering matrix that depend on the scattering angle θ and azimuth γ.

Then, for scattering of an electromagnetic wave by a spherical particle, taking into account the principle of reciprocity, expression (3) can be written as

$$(E_{|}^{refl}\ E_{\perp}^{refl}\ ) = \frac{e^{ik(r-z)}}{-ikr} (A_2\, 0\, 0\, A_1\ )(E_{|}^{inc}\ E_{\perp}^{inc}\ ), \tag{4}$$

where

$$A_1 = \frac{1}{2} \sum_n (2n+1)(a_n + b_n) ; \tag{5}$$

$$A_2 = \frac{1}{2} \sum_n^{n=\infty} (2n+1)(a_n + b_n)(\cos\cos\theta). \tag{6}$$

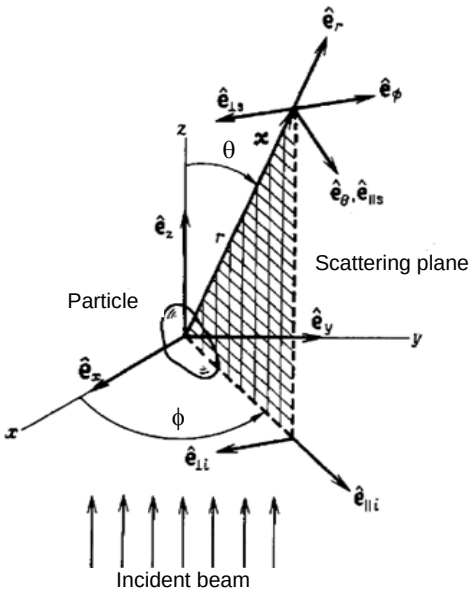

Fig. 2. Interaction processes

In formulas (5), (6), the coefficients of the scattering series a_n and b_n are found using the following expressions:

$$a_n = \frac{m\psi_n(mx)\psi'_n(\eta x) - \psi_n(mx)\psi'_n(mx)}{m\psi_n(mx)\xi'_n(x) - \xi_n(x)\psi'_n(mx)};$$

$$b_n = \frac{\psi_n(mx)\psi'_n(mx) - m\psi_n(mx)\psi'_n(mx)}{\psi_n(mx)\xi'_n(x) - m\xi_n(x)\psi'_n(mx)},$$

where $\psi_n(\eta x)$, $\xi_n(x)$ are the Riccati–Bessel functions, and x and m denote the diffraction parameter and relative refractive index, respectively.

Where in

$$x = ka = \frac{2\pi m_2 a}{\lambda}; \tag{7}$$

$$m = \frac{m_1}{m_2}, \tag{8}$$

where a is the particle radius, m_1 and m_2 are the refractive indices of the particle and medium (air), respectively.

We expand the functions included in the coefficients a_n and b_n in the power series and save only the terms of order x^6. The first four obtained coefficients are as follows:

$$a_1 = -\frac{i2x^3}{3}\frac{m^2-1}{m^2+2} - \frac{i2x^5}{5}\frac{(m^2-2)(m^2-1)}{(m^2+2)^2} + \frac{4x^6}{9}\left(\frac{m^2-1}{m^2+2}\right)^2;$$

$$b_1 = -\frac{ix^5}{45}(m^2-1); \quad a_2 = -\frac{ix^5}{15}\frac{m^2-1}{2m^2+3}; \quad b_1 \approx 0.$$

If $|m|x<1$, then $|b_1|<|a_1|$; under this assumption, the elements of the amplitude matrix up to terms of the order of x^3 are equal to

$$A_1\frac{3}{2}a\,, \tag{9}$$

$$A_2=\frac{3}{2}a_1\cos\cos\theta\,, \tag{10}$$

$$a_1=-\frac{i2x^3}{3}\frac{m^2-1}{m^2+2}\,. \tag{11}$$

From (4) follows the relation connecting the Stokes parameters of the incident and scattered electromagnetic waves:

$$(I_s\,Q_s\,U_s\,V_s\,)=$$

$$=\frac{1}{k^2r^2}(S_{11}\,S_{12}\,0\,0\,S_{12}\,S_{11}\,0\,0\,0\,0\,S_{33}\,S_{34}\,0\,0-S_{34}\,S_{33}\,)(I_i\,Q_i\,U_i\,V_i\,),$$

where

$$S_{11}=\frac{1}{2}(|S_2|^2+|S_1|^2),\;\; S_{12}=\frac{1}{2}(|S_2|^2-|S_1|^2)\,,$$

$$S_{33}=\frac{1}{2}(S_2^*S_1+S_2S_1^*)\,,\;\; S_{34}=\frac{i}{2}(S_1S_2^*-S_2S_1^*)\,.$$

In view of (9), (10), the scattering matrix for a spherical particle takes the form

$$\frac{9|a|^2}{4k^2r^2}\left(\frac{1}{2}(1+\theta)\frac{1}{2}(\theta-1)0\,0\,\frac{1}{2}(1-\theta)\frac{1}{2}(1+\theta)0\,0\,0\,0\cos\cos\theta\;\;0\,0\,0\,0\cos\cos\theta\;\right). \tag{12}$$

Note that if the incident electromagnetic wave of intensity I_0 is not polarized, then the law of Rayleigh scattering determines the intensity of the scattered wave from (12):

$$I=\frac{8\pi^4m_2a^6}{\lambda^4r^2}\left|\frac{m^2-1}{m^2+2}\right|^2(1+\theta\,)I_0\,.$$

The relationship between the rain intensity and the radius of the drops is conveniently represented as an empirical function of the average size distribution of raindrops, and written as follows:

$$F(a)=1-e^{-\left(\frac{a}{\alpha}\right)\cdot\eta}, \tag{13}$$

where the function $F(a)$ characterizes that part of the total volume of water that falls on drops of radius from 0 to a; η is the constant equal to 2.25.

The parameter α depends on the rain intensity I_r as listed below:

I_r, *mm / hour*	0.5	1.0	2.5	5.0	10	25
α	1.11	1.3	1.61	1.89	2.22	2.74

Determining the complex refractive index of water and metal object

The complex refractive index and the complex dielectric constant are related to each other as follows:

$$\varepsilon = \varepsilon' + i\varepsilon''; \quad \varepsilon = m^2; \tag{14}$$

$$m = n - i\chi, \tag{15}$$

where ε' is the real part of the complex dielectric constant and ε'' is the imaginary part of it, n is the refractive index, χ is the extinction coefficient.

From (14), (15) we obtain following expressions:

$$\varepsilon' = n^2 - \chi^2; \quad \varepsilon'' = 2n\chi;$$

$$n^2 = \frac{1}{2}\varepsilon'\left[1 + \sqrt{1 + \left(\frac{\varepsilon''}{\varepsilon'}\right)^2}\right]; \tag{16}$$

$$\chi = \frac{\varepsilon''}{2n}. \tag{17}$$

In order to use formulas (14) and (15) for calculating complex refractive index of water drop, we need to look at dipole theory.

According to the Debye dipole theory, the real part of the complex dielectric constant is expressed by the following formula:

$$\varepsilon' = n_0^2 + \frac{\varepsilon - n_0^2}{1 + \left(\frac{\lambda_s}{\lambda}\right)^2}, \tag{18}$$

and the imaginary part is

$$\varepsilon'' = \frac{\lambda_s}{\lambda}\frac{\varepsilon_0 - n_0^2}{1 + \left(\frac{\lambda_s}{\lambda}\right)^2}, \tag{19}$$

where n_0 is the optical refractive index, ε_0 is the permittivity of free space, λ is the wavelength, and λ_s is the so-called "shocks wave" which corresponds to the maximum value of the imaginary part of the dielectric constant.

Numerous measurements show that $\varepsilon_0 = 80.8$, $n_0^2 = 1.8$ and $\lambda_s = 1.6$. Above expressions allow to calculate complex refractive index for water drop.

For metal object, complex refractive index is often expressed as

$$m^2 = \varepsilon\mu\mu_0 = \left(\varepsilon' - \frac{i\sigma}{2\pi f\varepsilon_0}\right)\mu\mu_0, \tag{20}$$

where f is the wave frequency, σ is the relative conductivity of a material, μ is the relative permeability of a material, μ_0 is the magnetic permeability of free space, $\mu_0 = 1.2566 \cdot 10^{-6}$ H/m.

Neglecting the real part in (20), which is true for navigation radar frequencies, complex refractive index for metal objects is obtained as follows:

$$m = \sqrt{-\frac{i\sigma}{2\pi f \varepsilon_0}\mu\mu_0}\ . \tag{21}$$

Generalized Muller matrix for a composite target

Suppose that against the background of precipitation in the form of rain with intensity I_r, there is a navigational target, the radar cross-section (RCS) of which is less than or comparable with the total RCS of rain drops. In this case, expression (4) in Cartesian dimensions is written as follows:

$$(E_x^{refl}\ E_y^{refl}\ ) = \frac{e^{ik(r-z)}}{-ikr}\left[\sum_{l=1}^{N}(A_2\,0\,0\,A_1\ ) + (\Phi_1\,0\,0\,\Phi_2\ )\right]\times$$

$$\times(\cos\cos\gamma\ \sin\sin\gamma\ \sin\sin\gamma\ -\cos\cos\gamma)(E_{|}^{inc}\ E_{\perp}^{inc}\ )\,, \tag{22}$$

where N is the number of rain drops in the irradiated volume, γ is the azimuth.

It is easy to determine the number N from the considerations that in one cubic meter the number of raindrops and drizzle drops rarely exceeds 1000. Then for N we find,

$$N = 1000[V_{irr}] = 500\left[\pi\left(\frac{r^2\lambda^2}{4A}\right)c\tau\right],$$

where V_{irr} is the irradiated volume, A is the effective area of the radar antenna, c is the speed of light, τ is the duration of the probe pulse, and […] sign denotes ceiling function.

RESULTS AND DISCUSSION

Using formulas (7)–(11) and (13)–(19), we have estimated numeric values of refraction and extinction parameters as well as scattering coefficient a_1 for a typical rain drop sizes. Results are summarized in Table 1 for both *X*-band and *S*-band radar frequencies.

As expected, extinction and scattering rise with the carrier frequency. Within same wavelength, size of rain drop is directly proportional to the scattered wave amplitude.

Table 1. Influence of raindrop size on permittivity, refraction, extinction, and scattering coefficient for *X*-band and *S*-band radar frequencies

a, mm	a_1	λ, cm	ε'	ε''	ε	m_2
1.5	$3.794\cdot10^{-4} + 0.02i$	3	63.461	32.803	81	$8.213 - 1.997i$
2	$8.994\cdot10^{-4} + 0.047i$					
3	$3.035\cdot10^{-3} + 0.159i$					
1.5	$3.072\cdot10^{-6} + 5.379\cdot10^{-4}i$	10	79.023	12.324	81	$8.916 - 0.691i$
2	$7.282\cdot10^{-5} + 1.913\cdot10^{-3}i$					
3	$2.458\cdot10^{-5} + 4.564\cdot10^{-3}i$					

As an example, let us calculate the scattering matrix for 1 m^3 of rain drops with radius of 1.5 mm irradiated by plain wave with wavelength of 3 cm and scattering angle $\theta = 0^\circ$ over the time τ. Refractive index for air is $m_1 = 1$.

Muller matrix coefficients have been obtained as follows:

$$(I_s\ Q_s\ U_s\ V_s\ ) = \frac{1}{k^2 r^2}(892.526 - 0.04500 - \\ - 0.045892.5260000892.5260000892.526\ )(I_i\ Q_i\ U_i\ V_i\ ). \quad (23)$$

As can be seen from (23), scattering matrix has six nonzero elements, and only two independent ones. Since the main contribution is done by diagonal elements of the matrix, we can consider it diagonal.

Now, if radar beam will meet a metal object, the scattering matrix (23) will transform in new one:

$$(I_s\ Q_s\ U_s\ V_s\ ) = \frac{1}{k^2 r^2}(893.583 - 1.12600 - 1.126893.5830000891.58759.68400 - \\ - 59.684891.587\ )(I_i\ Q_i\ U_i\ V_i\ ). \quad (24)$$

Numerical values of Φ_1 and Φ_2 from (22) were obtained using formulas (20), (1) and (2). In (20), the relative conductivity was taken $\sigma = 7690000$ $\text{Ohm}^{-1}\text{m}^{-1}$, and the relative permeability of the metal material is $\mu = 100$ (carbon steel).

It can be seen from (24), another pair of nonzero elements has appeared. This suggests practical improvement of the navigation target detection method. By determining ellipsometric parameters of the scattered wave within radar's signal processing algorithm, target existence would be discovered easily.

For this purpose, circular polarized (CP) or $\pm 45^\circ$ polarized ($\pm 45^\circ$P) incident probing radiation is required. As can be seen from Table 2, CP and $\pm 45^\circ$P *X*-band probing results in zero values for azimuth and ellipticity irrespective to the rain intensity, if target is not available. However, presence of target results in nonzero values for those two parameters.

Table 2. Ellipsometric parameters of scattered circular and 45° polarized 3 cm waves at different environmental and navigational conditions

I_r, mm/hour		0.5	1	2.5	5
Rain	Azimuth (CP)	0	0	0	0
	Ellipticity (CP, ±45°P)	0	0	0	0
Rain + object	Azimuth (CP)	2	2.1	2.2	2.5
	Ellipticity (CP, ±45°P)	0.134	0.056	0.029	0.017

Improving navigation safety through statistical target detection in atmospheric precipitation involves the use of advanced radar technologies and data processing techniques. For Maritime Autonomous Ships (MAAS) in particular, this approach can significantly improve situational awareness and collision avoidance capabilities:

- Advanced radar systems. MAAS are equipped with advanced radar systems capable of operating in a variety of weather conditions, including rain and snow. These radars utilize special technologies to distinguish between real targets (such as other vessels) and interference caused by precipitation.
- Statistical signal processing. This method is based on statistical signal processing algorithms. These algorithms analyse radar signals and use statistical models to distinguish between real targets and interference caused by precipitation. Statistical models are created based on extensive data analysis and experimentation.

- Constant False Alarm Rate (CFAR). A key component of this method is the use of constant false alarm rate (CFAR) technology. CFAR algorithms dynamically adjust the target detection threshold based on the statistics of received radar signals. This maintains a constant false alarm rate even in the presence of interference.
- Probability Density Functions. In low resolution radars, the probability density function of interference often follows a Rayleigh distribution. For high resolution radars, the Weibull distribution may be more appropriate. These probability density functions are used to model the statistical behaviour of radar signals.
- Adaptive thresholding. The radar system continuously adapts its detection threshold depending on the prevailing environmental conditions. When heavy precipitation is detected, the system dynamically raises the detection threshold to screen out interference. This ensures that targets of interest remain visible.
- Integration with sensor fusion. Radar data processed using the statistical target detection method is integrated with data from other sensors on board the MAAS. These can be cameras, LiDAR, GPS and AIS (automatic identification system). This integration of data from multiple sensors increases overall situational awareness.
- Real-time decision-making. The processed information is fed into the MAAS decision-making algorithms. These include collision avoidance, route planning, and other navigation functions. When a potential collision hazard is detected, MAAS can autonomously take evasive action.
- Continuous Learning and Adaptation. Statistical models and algorithms are designed to learn and adapt over time. As MAAS encounters different environmental conditions and navigation scenarios, the system refines its statistical models to achieve even greater accuracy.

This enables MAAS to navigate safely even in unfavourable weather conditions where traditional radar systems may encounter interference from precipitation. The integration of statistical signal processing and CFAR techniques enhances MAAS' ability to accurately detect and respond to potential collision risks, which significantly improves navigation safety.

CONCLUSIONS

The findings presented in this study unveil a remarkable phenomenon in electromagnetic wave scattering: when a spherical raindrop is illuminated at different angles, there is an absence of depolarization in the incident wave. This stands in stark contrast to the partial depolarization exhibited by a metal target, resulting in distinct azimuth and ellipticity characteristics of the scattered wave. Leveraging this polarization contrast holds tremendous promise for advancing navigation radar technology, offering a notable boost in the precision and reliability of target detection.

One of the most significant merits of this method lies in its capability to facilitate target detection regardless of atmospheric precipitation intensity and the accompanying noise-to-signal ratio. This resilience stems from the invariant nature of the parameter, which remains unaffected by Radar Cross Section (RCS) variations.

However, it is important to note that the implementation of this method necessitates a navigation radar station equipped with at least two channels, specifi-

cally with horizontal polarization and 45° polarization. While this may entail increased costs and operational complexity for shipboard radar systems, the benefits in terms of heightened navigational security significantly outweigh this drawback, particularly in the realm of high-speed maritime transportation. The potential gains in safety and accuracy of navigation far outweigh the associated investment, marking a substantial step forward in maritime technology.

REFERENCES

1. Craig Bohren, Donald Huffman, *In Absorption and Scattering of Light by Small Particles*. 1983. doi: 10.1002/9783527618156
2. Yuxin Qin, Yu. Chen, "Signal processing algorithm of ship navigation radar based on azimuth distance monitoring," *International Journal of Metrology and Quality Engineering*, 2019. doi: 10. 12. 10.1051/ijmqe/2019010
3. V. Tatarinov, "Polarization Invariants of the Scattering Matrix and Stability of their Statistical Characteristics in the Aperture Synthesis Problem," *Proc. of the European Conference synthetic Aperture Radar, March 26 – 28, 1996, Königswinter, Germany*, pp. 113–115.
4. E. Luneburg, S.R. Cloude, and W.-M. Boerner, "On the proper polarimetric scattering matrix formulation of the forward propagation versus backscattering radar systems description," *IGARSS'97. 1997 IEEE International Geoscience and Remote Sensing Symposium Proceedings. Remote Sensing - A Scientific Vision for Sustainable Development, Singapore, 1997*, vol. 4, pp. 1591–1593. doi: 10.1109/IGARSS.1997.608965
5. Genwang Liu, Xi Zhang, and Junmin Meng, "A Small Ship Target Detection Method Based on Polarimetric SAR," *Remote Sensing*, 11(24), 2938, 2019. doi: 10.3390/rs11242938
6. Stanisław Rosłoniec, *Radiolocation and Its Basic Principles*. 2023. doi: 10.1007/978-3-031-10631-6_1
7. Jerry Jose, A. Rekh, and M.J. Jose, "Demonstrating Antenna Miniaturisation for Radiolocation Applications using Double Elliptical Patches," *Defence Science Journal*, 71, pp. 515–523, 2021. doi: 10.14429/dsj.71.16276
8. N. Ayuso et al., "A new radiolocation method for precise depth estimation and its application to the analysis of changes in groundwater levels in Colonia Clunia Sulpicia," *Archaeological Prospection*, vol. 29, issue 3, 2022. doi: 10.1002/arp.1858
9. Aleksander Droszcz, Konrad Jedrzejewski, Julia Kłos, Krzysztof Kulpa, and Mariusz Pożoga, "Beamforming of LOFAR Radio-Telescope for Passive Radiolocation Purposes," *Remote Sensing*, 13(4), 810, 2021. doi: 10.3390/rs13040810
10. Douglas N. Travers, M. Pike Castles, and William M. Sherrill, "Radiolocation Experiments in an Urban Environment," *IEEE Transactions on Electromagnetic Compatibility*, vol. EMC-12, issue 4, pp. 174–177, 1970. doi: 10.1109/TEMC.1970.303054
11. Danko Antolovic, "Directional radio response of a 802.11b device guided by radiolocation," *PORTABLE-POLYTRONIC 2008 - 2nd IEEE International Interdisciplinary Conference on Portable Information Devices and the 2008 7th IEEE Conference on Polymers and Adhesives in Microelectronics and Photonics*. doi: 10.1109/PORTABLEPOLYTRONIC.2008.4681258
12. Danko Antolovic, "An Algorithm for Simultaneous Radiolocation of Multiple Sources," *2009 IEEE 70th Vehicular Technology Conference Fall*, pp. 1–5. doi: 10.1109/VETECF.2009.5378896
13. Nanjing Yu, Haohao Ren, Tianmin Deng, and Xiaobiao Fan, "A Lightweight Radar Ship Detection Framework with Hybrid Attentions," *Remote Sensing*, 15, 2743, 2023. doi: 10.3390/rs15112743
14. Mikhail Popov, Sergey Stankevich, Valentyn Pylypchuk, Kun Xing, and Chunxiao Zhang, *Unified Approach to Inshore Ship Detection in Optical/radar Medium Spatial Resolution Satellite Images*. 2023. doi: 10.1007/978-981-99-4098-1_8

15. Xueqian Xu, Bing Wu, Lei Xie, A.P. Teixeira, and Xinping Yan, "A Novel Ship Speed and Heading Estimation Approach Using Radar Sequential Images," *IEEE Transactions on Intelligent Transportation Systems*, pp. 1–14, 2023. doi: 10.1109/TITS.2023.3281547
16. Zhe Chen, Zhiquan Ding, Xiaoling Zhang, Xiaoting Wang, and Yuanyuan Zhou, "Inshore Ship Detection Based on Multi-Modality Saliency for Synthetic Aperture Radar Images," *Remote Sensing*, 15, 3868, 2023. doi: 10.3390/rs15153868
17. Yongsheng Zhou, Hanchao Liu, Fei Ma, Zongxu Pan, and Fan Zhang, "A Sidelobe-Aware Small Ship Detection Network for Synthetic Aperture Radar Imagery," *IEEE Transactions on Geoscience and Remote Sensing*, pp. 1-1, 2023. doi: 10.1109/TGRS.2023.3264231
18. Tianyi Zhang, Shujiang Liu, Zegang Ding, Yongpeng Gao, and Kaiwen Zhu, "A Motion State Judgment and Radar Imaging Algorithm Selection Method for Ship," *IEEE Transactions on Geoscience and Remote Sensing*, 60, pp. 1–18, 2022. doi: 10.1109/TGRS.2022.3212674
19. Alain Protat, Valentin Louf, Joshua Soderholm, Jordan Brook, and William Ponsonby, "Three-way calibration checks using ground-based, ship-based, and spaceborne radars," *Atmospheric Measurement Techniques*, 15, pp. 915–926, 2022. doi: 10.5194/amt-15-915-2022
20. Zhuolin Wang, Yingjun Zhang, "Estimation of ship berthing parameters based on Multi-LiDAR and MMW radar data fusion," *Ocean Engineering*, 266, 113155, 2022. doi: 10.1016/j.oceaneng.2022.113155
21. O. Melnyk, Y. Bychkovsky, and A. Voloshyn, "Maritime situational awareness as a key measure for safe ship operation," *Scientific Journal of Silesian University of Technology. Series Transport*, 114, pp. 91–101, 2022. doi: https://doi.org/10.20858/sjsutst.2022.114.8
22. S. Onyshchenko, O. Melnyk, "Efficiency of Ship Operation in Transportation of Oversized and Heavy Cargo by Optimizing the Speed Mode Considering the Impact of Weather Conditions," *Transport and Telecommunication*, 23 (1), pp. 73–80, 2022. doi: 10.2478/ttj-2022-0007
23. O. Melnyk et al., "Autonomous Ships Concept and Mathematical Models Application in their Steering Process Control," *TransNav*, 16 (3), pp. 553–559, 2022. doi: 10.12716/1001.16.03.18
24. O. Melnyk, S. Onyshchenko, "Navigational safety assessment based on Markov-model approach," *Scientific Journal of Maritime Research*, 36 (2), pp. 328–337, 2022. doi: https://doi.org/10.31217/p.36.2.16
25. O. Melnyk, S. Onyshchenko, O. Onishchenko, O. Lohinov, and V. Ocheretna, "Integral approach to vulnerability assessment of ship's critical equipment and systems," *Transactions on Maritime Science*, 12(1), 2023. doi: 10.7225/toms.v12.n01.002
26. O. Melnyk et al., "Review of Ship Information Security Risks and Safety of Maritime Transportation Issues," *TransNav*, vol. 16, no. 4, pp. 717–722, 2022. doi: 10.12716/1001.16.04.13
27. O. Melnyk et al., "Study of Environmental Efficiency of Ship Operation in Terms of Freight Transportation Effectiveness Provision," *TransNav*, vol. 16, no. 4, pp. 723–729, 2022. doi: 10.12716/1001.16.04.14
28. O. Melnyk et al., "Application of Fuzzy Controllers in Automatic Ship Motion Control Systems," *International Journal of Electrical and Computer Engineering*, vol. 13, no. 4, pp. 3958–3968, 2023. doi: 10.11591/ijece.v13i4.pp3948-3957
29. Y. Volyanskaya, S. Volyanskiy, A. Volkov, and O. Onishchenko, "Determining energy-efficient operation modes of the propulsion electrical motor of an autonomous swimming apparatus," *Eastern-European Journal of Enterprise Technologies*, 6 (8-90), pp. 11–16, 2017. doi: 10.15587/1729-4061.2017.118984
30. V.A. Golikov, V.V. Golikov, Y. Volyanskaya, O. Mazur, and O. Onishchenko, "A simple technique for identifying vessel model parameters," *IOP Conference Series: Earth and Environmental Science*, 172 (1), art. no. 012010, 2018. doi: 10.1088/1755-1315/172/1/012010

31. V. Budashko, V. Nikolskyi, O. Onishchenko, and S. Khniunin, "Decision support system's concept for design of combined propulsion complexes," *Eastern-European Journal of Enterprise Technologies*, 3 (8-81), pp. 10–21, 2016. doi: 10.15587/1729-4061.2016.72543
32. V. Budashko, T. Obniavko, O. Onishchenko, Y. Dovidenko, and D. Ungarov, "Main Problems of Creating Energy-efficient Positioning Systems for Multipurpose Sea Vessels," *2020 IEEE 6th International Conference on Methods and Systems of Navigation and Motion Control, MSNMC 2020 - Proceedings*, art. no. 9255514, pp. 106–109, 2020. doi: 10.1109/MSNMC50359.2020.9255514
33. V. Piterska, D. Lohinov, and L. Lohinova, "Risk Management Mechanisms in Higher Education Institutions Based on the Information Support of Innovative Projects," *International Scientific and Technical Conference on Computer Sciences and Information Technologies, 2022-November*, pp. 410–413, 2022. doi: 10.1109/CSIT56902.2022.10000551
34. V. Piterska, A. Shakhov, O. Lohinov, and L. Lohinova, "The Method of Human Resources Management of Educational Projects of Institution of Higher Education," *International Scientific and Technical Conference on Computer Sciences and Information Technologies*, 2, art. no. 9321912, pp. 123–126. doi: 10.1109/CSIT49958.2020.9321912
35. Alla Bondar, Natalija Bushuyeva, Sergey Bushuyev, and Svitlana Onyshchenko, "Modelling of Creation Organisational Energy-Entropy," *International Scientific and Technical Conference on Computer Sciences and Information Technologies*, 2, art. no. 9321997, pp. 141–145, 2020. doi: 10.1109/CSIT49958.2020.9321997
36. S. Onyshchenko, A. Bondar, V. Andrievska, N. Sudnyk, and O. Lohinov, "Constructing and exploring the model to form the road map of enterprise development," *Eastern-European Journal of Enterprise Technologies*, 5 (3-101), pp. 33–42, 2019. doi: 10.15587/1729-4061.2019.179185
37. S. Bushuyev, S. Onyshchenko, N. Bushuyeva, and A. Bondar, "Modelling projects portfolio structure dynamics of the organization development with a resistance of information entropy," *International Scientific and Technical Conference on Computer Sciences and Information Technologies*, 2, pp. 293–298, 2021. doi: 10.1109/CSIT52700.2021.9648713
38. A. Bondar, S. Onyshchenko, O. Vishnevska, D. Vishnevskyi, S. Glovatska, and A. Zelenskyi, "Constructing and investigating a model of the energy entropy dynamics of organizations," *Eastern-European Journal of Enterprise Technologies*, 3 (3-105), pp. 50–56, 2020. doi: 10.15587/1729-4061.2020.206254
39. O. Scherbina, O. Drozhzhyn, O. Yatsenko, and O. Shybaev, "Cooperation forms between participants of the inland waterways cargo delivery: a case study of the dnieper region," *Scientific Journal of Silesian University of Technology. Series Transport*, 103, pp. 155–166, 2019. doi: 10.20858/sjsutst.2019.103.12
40. A. Shibaev, S. Borovyk, and I. Mykhailova, "Developing a strategy for modernizing passenger ships by the optimal distribution of funds," *Eastern-European Journal of Enterprise Technologies*, 6 (3-108), pp. 33–41, 2020. doi: 10.15587/1729-4061.2020.219293
41. M. Stetsenko et al., "Improving Navigation Safety by Utilizing Statistical Method of Target Detection on the Background of Atmospheric Precipitation" *Trends in Sustainable Computing and Machine Intelligence - Proceedings of ICTSM 2023*. doi: https://doi.org/10.1007/978-981-99-9436-6_8
42. P.M. Paithane, S.J. Wagh, "Novel modified kernel fuzzy c-means algorithm used for cotton leaf spot detection," *System Research and Information Technologies*, no. 4, pp. 85–99, 2023. doi: 10.20535/SRIT.2308-8893.2023.4.07
43. V. Sharma, S.S. Samant, "A multi-level decision-making framework for heart-related disease prediction and recommendation," *System Research and Information Technologies*, no. 4, pp. 7–20, 2023. doi: 10.20535/SRIT.2308-8893.2023.4.01
44. N.R. Kondratenko, O.O. Snihur, and R.M. Kondratenko, "Interval type-2 generalizing fuzzy model for monitoring the states of complex systems using expert knowl-

edge," *System Research and Information Technologies*, no. 2, pp. 63–73, 2023. doi: 10.20535/SRIT.2308-8893.2023.2.05

45. E.M. Kiseleva, O.M. Prytomanova, and L.L. Hart, "Application of optimal set partitioning theory to solving problems of artificial intelligence and pattern recognition," *System Research and Information Technologies*, no. 4, pp. 91–101, 2021. doi: 10.20535/SRIT.2308-8893.2021.4.07

Received 02.11.2023

INFORMATION ON THE ARTICLE

Maksym S. Stetsenko, ORCID: 0000-0001-8155-2947, National University "Odesa Maritime Academy", Ukraine

Oleksiy M. Melnyk, ORCID: 0000-0001-9228-8459, Odesa National Maritime University, Ukraine, e-mail: m.onmu@ukr.net

Igor I. Vorokhobin, ORCID: 0000-0001-7066-314X, National University "Odesa Maritime Academy", Ukraine

Dmytro V. Korban, ORCID: 0000-0002-6798-2526, National University "Odesa Maritime Academy", Ukraine

Oleg A. Onishchenko, ORCID: 0000-0002-3766-3188, National University "Odesa Maritime Academy", Ukraine

Valentin B. Ternovsky, ORCID: 0000-0002-4402-4157, Odesa National Maritime University, Ukraine

Iryna M. Ivanova, ORCID: 0000-0002-1751-7781, Odesa National Maritime University, Ukraine

ВИКОРИСТАННЯ ПОЛЯРИЗАЦІЙНОГО ПІДХОДУ ДО ВИЯВЛЕННЯ ЦІЛЕЙ З МЕТОЮ ПІДВИЩЕННЯ ЕФЕКТИВНОСТІ ІДЕНТИФІКАЦІЇ МАЛИХ НАДВОДНИХ ОБ'ЄКТІВ ТА ЗАБЕЗПЕЧЕННЯ БЕЗПЕКИ СУДНОПЛАВСТВА / М.С. Стеценко, О.М. Мельник, І.І. Ворохобін, Д.В. Корбан, О.А. Онищенко, В.Б. Терновський, І.М. Іванова

Анотація. Досліджено новаторський підхід, що дає змогу значно підвищити ефективність навігаційних радіолокаційних станцій за несприятливих погодних умов. Традиційні суднові радари, які використовують горизонтальну поляризацію, стикаються з труднощами в ефективному придушенні дощових перешкод. Запропоновано інноваційний метод, що використовує кругову поляризацію для виявлення навігаційних цілей. Цей метод використовує відмінні поляризаційні властивості, які демонструють стабільні навігаційні цілі і флуктуаційні об'єкти, що заважають. Теоретичний аналіз і модельні експерименти обгрунтовують узгоджені значення параметра еліптичності розсіяних хвиль, незалежні від інтенсивності дощу, як для дощових перешкод, так і для поверхневих металевих об'єктів. Практичні наслідки таких досліджень є дуже перспективними, адже вони уможливлюють виявлення об'єктів незалежно від співвідношення шум/сигнал шляхом інтегрування додаткового каналу циркулярно поляризованих хвиль і застосування простих математичних функцій. Такий підхід знаменує собою значний крок до подолання проблем ідентифікації малих надводних об'єктів, пов'язаних із метеорологічними умовами в морських навігаційних радіолокаційних системах.

Ключові слова: безпека судноплавства, навігаційна безпека, морські перевезення, радіолокаційні перешкоди, несприятливі погодні умови, придушення перешкод, навігаційні цілі, автономні надводні транспортні засоби, принципи радіолокації, виявлення суден, точність радіолокації.